Available online at www.sciencedirect.com
ScienceDirect
Journal of Solid State Chemistry 179 (2006) 3981–3988
JOURNAL OF SOLID STATE CHEMISTRY
www.elsevier.com/locate/jssc

A new approach for the synthesis of K^+-free nickel hexacyanoferrate

Irene Carpani[a], Marco Giorgetti[a], Mario Berrettoni[a], Pier Luigi Buldini[b], Massimo Gazzano[c], Domenica Tonelli[a,*]

[a]*Dipartimento di Chimica Fisica e Inorganica, Università di Bologna, INSTM, UdR Bologna, Viale Risorgimento 4, 40136 Bologna, Italy*
[b]*CNR-ISTEC, Via Granarolo 64, 48018 Faenza (RA), Italy*
[c]*ISOF-CNR, Via Selmi 2, 40126 Bologna, Italy*

Received 13 April 2006; received in revised form 23 August 2006; accepted 10 September 2006
Available online 16 September 2006

Abstract

A Ni, Al hydrotalcite-like compound (Htlc) has been proven an useful host material for an alternative synthesis of a K^+-free mixed hexacyanoferrate $Ni_{1.5}Fe^{III}(CN)_6$, which is very difficult to obtain in bulk. The first stage of the procedure consists in the intercalation of hexacyanoferrate(III) inside the Htlc structure. The intercalated Htlc has been treated with a $NiNO_3$ solution. The obtained material has been characterized by XRD, XAS Raman and FT-IR spectroscopy. The voltammetric response of the compound obtained after the complete solubilization of the Htlc host shows a typical fingerprint of nickel hexacyanoferrate material with a very low level of potassium. Elemental analysis confirmed the absence of K^+ and thus the occurrence of K^+-free nickel hexacyanoferrate (14% yield).

Keywords: K^+-free nickel hexacyanoferrate; Ni, Al double-layered hydroxide; Intercalation

1. Introduction

Layered double hydroxides (LDHs) or hydrotalcite-like compounds (Htlcs) are also known as anionic clays, due to their layered structure with a charge opposite to that of cationic clays. Their structural chemistry is based on that of magnesium hydroxide, brucite, where partial M^{II}/M^{III} substitution has taken place, resulting in a net positive charge which is compensated by interlayer anions or anionic complexes [1]. Their general formula, hereafter abbreviated as $M(II)/M(III)$-A, is $[M(II)_{1-x}M(III)_x(OH)_2]^{x+}A_{x/n}{}^{n-}\cdot mH_2O$ where $M(II)$ and $M(III)$ are the divalent and trivalent cations and A^{n-} is the interlayer anion.

A peculiarity of these compounds is their anion exchange feature, which enables the synthesis of a continuous growing family of new layered materials and sometimes represents the only alternative to incorporate a desired compound or to increase the loading of a particular metal [2].

Solid metal cyanometallates such as Prussian Blue and its analogues are of much interest since they exhibit both ionic conductivity as well as redox properties [3]. They constitute a class of fairly well-defined zeolite-like polynuclear inorganic materials with fixed metal ionic redox centres and freely diffusing cations in and out of the lattice structure, during the redox processes, in order to maintain electroneutrality. Investigating redox behaviour and dynamics of charge transport in thin films of such systems is important for understanding their interesting physical and chemical properties which make these compounds attractive for technical and analytical applications.

Recently, metal cyanometallates have found applications in electrochromism [4–7], electrocatalysis [8–10], solid-state batteries [11–14], ion-sieving membranes [15] molecular magnetism [16–19], ion-exchange selectivity [20–22] and corrosion protection [23]. Furthermore, their ion-exchange characteristics have made them attractive to develop sensors and biosensors [24–27].

While the redox behaviour of the various metal hexacyanoferrates are clearly related, they are dissimilar in many respects [28]. Among metal hexacyanoferrates, nickel(II) hexacyanoferrate(II,III), NiHCF can

*Corresponding author. Fax: +39 0512093690.
E-mail address: domenica.tonelli@unibo.it (D. Tonelli).

0022-4596/$ - see front matter © 2006 Elsevier Inc. All rights reserved.
doi:10.1016/j.jssc.2006.09.004

be considered as a model system for fundamental and applied studies since both oxidized and reduced forms of NiHCF allow an easy transport of supporting electrolyte cations while providing charge electroneutrality during the redox processes and, therefore, this material displays two reversible and reproducible voltammetric peak systems not only in K^+ containing electrolytes, but also in the presence of other alkali metal cations. Furthermore, NiHCF can be formed as a thin film on many conductive materials by several synthetic routes [29–31].

In bulk synthesis, processing conditions can be used to tune the stoichiometry of NiHCF powders over the entire range of Ni:Fe stoichiometries and recently Steen and Schwartz have reported that bulk methods can be adapted to thin film synthesis [32].

In a previous work [33] we reported a study on the intercalation kinetics of $Fe(CN)_6^{4-}$ into a Ni/Al–Cl. The study was performed also to search a new approach for the synthesis of a pure mixed hexacyanoferrate $[Ni_2Fe^{II}(CN)_6]$, i.e., without the presence of K^+ as counter cations, which is very difficult to obtain. The rationale was to destroy the intercalated Htlc by keeping it in contact with a Ni^{2+} solution. Actually, the compound $[Ni_2Fe^{II}(CN)_6]$ was not synthesized due to the intercalation of the hexacyanoferrate(II) as ion-pair with potassium.

Since hexacyanoferrate(III) is characterized by a lower charge density and different chemical interactions with the hydrotalcite structure [2], we have carried out the intercalation of $Fe(CN)_6^{3-}$ into the same Htlc and tried to synthesize the K^+-free nickel hexacyanoferrate compound $Ni_{1.5}[Fe^{III}(CN)_6]$, following the same procedure [33]. Also this time the synthesis did not lead to the K^+-free nickel hexacyanoferrate.

Since the results obtained from FT-IR, Raman spectra and the XRD pattern of the Htlc intercalated with hexacyanoferrate(III) did not exclude the possibility that the K^+-free nickel hexacyanoferrate could be present inside the Htlc host, we exploited the different solubility of the host/guest compounds in acid media to verify this hypothesis. From XRD, electrochemical behaviour and elemental analysis, the solid residue obtained from the solubilization of the Htlc host in HCl, resulted to be the desired $Ni_{1.5}[Fe^{III}(CN)_6]$.

2. Experimental

2.1. Synthesis of the compounds

The starting material Ni/Al–Cl was synthesized following the co-precipitation method described by Miyata, by using freshly boiled double distilled water for the preparation of the solutions and working under nitrogen atmosphere to avoid the contamination from carbon dioxide [34]. All salts were ACS reagent grade. Hydrated metal salts $AlCl_3 \cdot 6H_2O$, $NiCl_2 \cdot 6H_2O$ and $K_3Fe(CN)_6$ were as supplied by Aldrich and Fluka. Standard solutions of 1.0 M NaOH were supplied by Merck.

The intercalation of the anion $Fe(CN)_6^{3-}$ was performed by the exchange method. About 0.4 g of Htlc was suspended in 20.0 mL of water and magnetically stirred for 2 h under a high purity nitrogen flow. Then 1.5 mL of 0.4 M $K_3Fe(CN)_6$ aqueous solutions, corresponding to a $Fe(CN)_6^{3-}/Al^{3+}$ molar ratio of 2.5:1, were added; the nitrogen flow was stopped and the reaction container was sealed in order to maintain an inert atmosphere. After a 9 h exchanged time chosen on the basis of previous results [33], the solid obtained (Htlc Ni/Al–$Fe^{III}(CN)_6$) was separated by centrifugation, repeatedly washed with double distilled water and finally dried in an oven at 50 °C, under vacuum. Later an amount of the intercalated Htlc was suspended, under magnetic stirring, in a 0.1 M Ni^{2+} solution for 24 h. The solid obtained $X_yNi_xFe^{III}(CN)_6$ was separated by centrifugation, dried under vacuum in an oven (50 °C) and characterized by means of, XRD, FT-IR, Raman and X-ray absorption spectroscopy and cyclic voltammetry.

2.2. Elemental analysis ICP-OES

Fe, Ni and K were determined with a Varian (Palo Alto, CA_USA) Liberty 200 sequential ICP-OES, equipped with a 1800 grooves mm^{-1} holographic grating, a 0.75 m focal length Czerny-Turner optical system, a V-groove nebulizer, a Sturman-Master inert nebulization chamber and a standard radial quartz torch (injector ID 1.4 mm). The RF generator is based on a 40.68 MHz crystal-controlled oscillator. The instrument was optimized for the viewing height, scan and search windows, power, plasma flow, auxiliary plasma flow, pump speed and nebulizer pressure. Dynamic background correction was used for all the wavelengths in the determination. Analytical lines were 231.604(II) nm for Ni, 259.940(II) nm for Fe and 766.490 for K. Overall sample dilution was 1:20 in 1 M HCl (or 1 M LiOH for the material solubilized after HCl treatment). The analytical blank was analysed for each dissolution mixture to correct for any contaminant present. In addition, the samples were analysed using standards prepared in either 1 M HCl or 1 M LiOH, as required.

2.3. Electrochemical test

Cyclic voltammetry (CV) was carried out with a CHInstruments (Austin, TX, USA) model 660A analyzer. The experiments were performed in the 0–0.8 V potential range, in a conventional three-electrode cell, using a Pt wire as counter electrode. The working electrode was constituted by a paraffin-impregnated graphite, sandwiched in a Pt net as current collector, containing the $X_yNi_xFe^{III}(CN)_6$ powder or by a gold disk with the $Ni_{1.5}[Fe^{III}(CN)_6]$ powder mechanically attached.

All the measurements were carried out at room temperature (approx. 22 °C) and high purity nitrogen was used to deoxygenate the solutions. All potentials were recorded versus a saturated calomel electrode (SCE).

2.4. X-ray diffraction

X-ray powder diffraction patterns were recorded, in the 2θ range of 5–80°, on a Philips PW 1050/81 X-ray powder diffractometer equipped with a graphite monochromator and a vertical goniometer, using Cu$K\alpha$ radiation (1.5406 Å) and a scanning rate of 0.05°/s.

2.5. FT-IR spectra

The Fourier-transform infrared spectra (FT-IR) were recorded in a Nicolet Nexus 470 spectrometer, configured with a Nicolet Continuum microscope and a MCT/B liquid-nitrogen cooled detector. Spectra were collected in attenuated total reflectance (ATR) mode, through a Cassegrain objective (14 ×) reaching a spatial resolution of $\sim$100 μm^2. The samples were investigated without any pre-treatment by putting in intimate contact the silicon crystal with the powder. The spectra were recorded (as sum of 256 scans with a resolution of 4 cm^{-1}) in the spectral region of the medium infrared (500–4000 cm^{-1}).

2.6. Raman spectra

A Renishaw Raman System RM1000 was employed to perform Raman analyses in the range between 2000 and 2500 cm^{-1}. It was configured with a Leica DMLM microscope (with 5 ×, 20 ×, 50 × and 20 × LD objectives), a notch filter, and a charge-coupled device (CCD) thermoelectrically cooled (203 K) detector. An argon ion laser (514.5 nm) and a diode laser (780.0 nm) were used as radiation sources, with a nominal laser power varied from 10 to 25 mW. In a typical Raman experiment, the laser was focused on the sample with the help of an objective lens; in all cases a 50 × objective was employed. In order to obtain a satisfactory signal-to-noise ratio, the time of each scan was 10 s and the total number of scans from 2 to 10. Spectra were calibrated using the 520 cm^{-1} Raman line of a silicon wafer.

2.7. XAS data collection

X-ray absorption experiments (XAS) were performed at the Synchrotron Radiation Source (SRS) at Daresbury Laboratory, Warrington, England using the beam line 7.1.

The storage ring operates at 1.6 GeV with a typical current of 240 mA. A Si (111) double crystal monochromator was employed. In order to reduce higher harmonics, the second crystal was detuned at about 70%. Internal references for energy calibration were used for iron and nickel. Data at the Fe K-edge were acquired in fluorescence mode using a Ge high-purity, 13-element solid-state detector and in transmission mode at the Ni K-edge. XAS spectra were collected in the k (Å^{-1}) space up to $k = 15$ at 0.03 k intervals with a 3 s integration time allowing extended X-ray absorption fine structure (EXAFS) spectra to be recorded sequentially after the near edge X-ray absorption structure (XANES) region. Samples were prepared by mixing powdered compounds with cellulose (Merck) (20:80 w/w) and applying a pressure of about 5 tons cm^{-2} in order to obtain a pellet.

2.8. XAS data analysis

XANES spectra were normalized to an edge jump of unity. A prior removal of the background absorption was done by subtraction of a linear function extrapolated from the pre-edge region. The EXAFS analysis was performed using the GNXAS package [35,36] which takes into account Multiple Scattering (MS) theory. The method is based on the decomposition of the EXAFS signals into a sum of several contributions, the n-body terms. It allows the direct comparison of the raw experimental data with a model theoretical signal. The procedure avoids any filtering of the data and allows a statistical analysis of the results. The theoretical signal is calculated ab initio and contains the relevant two-body $\gamma^{(2)}$ and the three-body $\gamma^{(3)}$ multiple scattering (MS) terms. The two-body terms are associated with pairs of atoms, probing their distances and variances. The three-body terms are associated with triplets of atoms and probe angles, bond–bond, and bond–angle correlations. Data analysis is performed by minimizing a χ^2-like function, which compares the theoretical model to the experimental signal. The phase shifts for the photoabsorber and backscatterer atoms were calculated ab initio starting from the structural model previously reported [37]. They were calculated according to the muffin-tin approximation. The Hedin–Lundqvist complex potential [38] was used for the exchange-correlation potential of the excited state. The core hole lifetime, Γ_c, was fixed to the tabulated value [39] and included in the phase shift calculation. The experimental resolution used in the fitting analysis was about 2 eV, in agreement with the stated value for the beam line used. The values of S_0^2 were found to be between 0.82 and 0.86 for the Fe. The relevant E_0's values were found to be displaced by several eV with respect to the edge inflection point. The fitting procedure at the Fe K-edge was conducted taking into account the relevant set of multiple scattering paths [37]. Hence, we have included in the fitting procedures the two-atom contributions $\gamma_1^{(2)}$ Fe–C with degeneracy of 6, and the three-body contribution $\eta_1^{(3)}$ Fe–C–N, where the $\eta_1^{(3)}$ Fe–C–N includes both $\gamma^{(2)}$ Fe–N and $\gamma^{(3)}$ Fe–C–N contribution. It is worth to point out that the inclusion of the three-body term $\eta_1^{(3)}$ allowed to monitor the shells beyond the second one by using the same three-atom coordinates both for the two-atom and the three-atom contributions. The overall number of parameters included in the fitting procedure was 9:2 bond distances, 1 angle, 3 EXAFS Debye-Waller factors and three non-structural terms: E_0, S_0^2 and the experimental resolution.

3. Results and discussion

3.1. Characterization of $X_yNi_xFe^{III}(CN)_6$

3.1.1. X-ray diffraction

From the XRD data obtained previously for the parent and the intercalated Ni/Al–$Fe^{III}(CN)_6$ [33] we concluded that the insertion of hexacyanoferrate(III) ions induced a not complete exchange of the native chloride. In fact, the pattern showed an increase of the interlayer spacing typical of the hexacyanoferrate-containing hydrotalcites, but also the typical reflections of the pristine Htlc.

The XRD pattern of $X_yNi_xFe^{III}(CN)_6$ (Fig. 1) displays the diffraction maxima typical of the parent Htlc at 11.1, 22.8, 35.0 (marked with a triangle), due to diffraction by basal planes (003), (006), (009), and a doublet close to 60°(2θ) due to the diffraction by the basal plane (110) [40]. The presence of these reflections reveals that chloride anions are still present after the overall process (intercalation of $Fe(CN)_6^{3-}$ and successive immersion in Ni^{2+} solution).

In addition 6 maxima (marked with an asterisk) assigned to a non-hydrotalcitic phase were observed. Taking into account the data reported in the literature (Table no. 46-0906, International Centre of Diffraction Data, 12 Campus Boulevard, Newton Square, PA 19073-3273, USA), the 2θ positions of these peaks can be attributed to the diffraction by basal planes (200), (220), (420), (440), (600), (620), typical of the compounds $KNiFe^{III}(CN)_6$ or $Ni_3[Fe(CN)_6]_2 \cdot 10H_2O$. This fact provides evidence for nickel hexacyanoferrate formation, obtained by reaction of the intercalated $Fe(CN)_6^{3-}$ with nickel ions.

3.1.2. FT-IR and Raman spectra

The IR spectrum of the compound $X_yNi_xFe^{III}(CN)_6$, in the region 2000–2250 cm^{-1}, is shown in Fig. 2. A broad band at 2100 cm^{-1} and another at 2167 cm^{-1} are present. Those bands are also present in $KNiFe^{III}(CN)_6$ or $HNiFe^{III}(CN)_6$ and can be attributed to the CN stretching of the above compounds, synthesized by simple mixing of a soluble Ni salt and $K_3Fe(CN)_6$ or $H_3Fe(CN)_6$, by comparison with their IR spectra (Fig. 2). A close inspection of the relative intensities of the two peaks suggests that potassium ion might be in the $X_yNi_xFe^{III}(CN)_6$ compound.

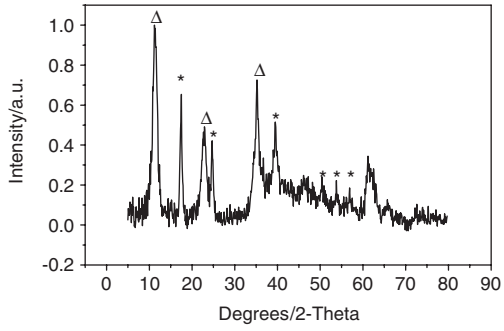

Fig. 1. XRD pattern of $X_yNi_xFe^{III}(CN)_6$. Triangle marks are assigned to the Ni/Al–Cl Htlc. Asterisk marks are assigned to the $KNiFe^{III}(CN)_6$ or $Ni_3[Fe(CN)_6]_2 \cdot 10H_2O$.

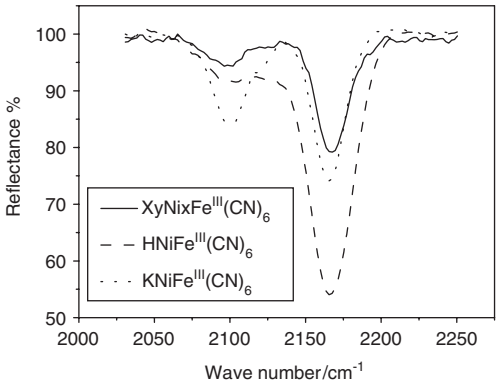

Fig. 2. FT-IR spectra of $KNiFe^{III}(CN)_6$ (dot line), $HNiFe^{III}(CN)_6$ (dash line) and $X_yNi_xFe^{III}(CN)_6$ (solid line).

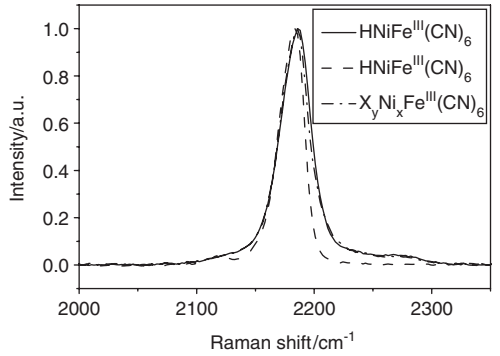

Fig. 3. Raman spectra of $KNiFe^{III}(CN)_6$ (dash line), $HNiFe^{III}(CN)_6$ (solid line) and $X_yNi_xFe^{III}(CN)_6$ (dot line).

The Raman spectrum of $X_yNi_xFe^{III}(CN)_6$, in the region 2000–2350 cm^{-1}, is displayed in Fig. 3, together with the spectra of $KNiFe^{III}(CN)_6$ and $HNiFe^{III}(CN)_6$. The curves are characterized by a strong band at 2187 cm^{-1} and a very weak one at 2118 cm^{-1} attributed to ν(CN) of the nickel hexacyanoferrate(III) compound [41]. Hence, the combined FT-IR and Raman analysis indicates that both $KNiFe^{III}(CN)_6$ and $HNiFe^{III}(CN)_6$ are most likely involved, thought the present data do not permit to discriminate between the two options. Besides, their presence were already observed in the FT-IR and Raman spectra of the Ni/Al–$Fe^{III}(CN)_6$ [42], even if the XRD pattern did not reveal the presence of their typical diffraction maxima, probably because the crystalline domains were too small to be observed.

The absence of the bands due to the CN stretching of ferrocyanide and ferricyanide intercalated in the Htlc layers confirms the XRD results: Ni^{2+} ions from the solution combines with $Fe(CN)_6^{3-}$ ions intercalated during the first stage of synthesis, leading to a mixed hexacyanoferrate compound.

3.1.3. X-ray absorption spectroscopy

In order to obtain structural information on both Ni/Al–$Fe^{III}(CN)_6$ and $X_yNi_xFe^{III}(CN)_6$, we acquired X-ray Absorption spectra. The technique is strongly sensitive to the short range environment of a selected metal and can be applied to disordered, amorphous and crystalline materials [43]. In particular, XAS applications in the field of the intercalation science have been proved to be very fruitful [44–46]. In this application, both Fe and Ni site could be monitored by XAS. Spectra taken at the Fe *K*-edge permit the study of the chemical environment of the guest, i.e.: the nickel hexacyanoferrate whereas recording spectra at the Ni *K*-edge are most likely related to the chemical environment of the host, the Htlc structure. In fact, in spite of the presence of the nickel hexacyanoferrate into the host, which adds a second Ni site, its relative concentration is very small and hence the overall XAS signal is due almost completely to the host. This issue is confirmed experimentally by the comparison of XANES spectra or Fourier Transform curves of parent Ni/Al–Cl and hexacyanoferrate(III)-intercalated Ni/Al–Cl Htlc compounds [42]. In fact, the curves in both sets of data are equivalent, providing evidence that only the Ni site related to the Htlc structure is probed while recording XAS data at the Ni edge. This fact has two implications. First, the occurrence of the nickel hexacyanoferrate compound can be only checked out by looking at the Fe *K*-edge measurements. Second, due to the relative low concentration of iron atoms in both Ni/Al–$Fe^{III}(CN)_6$ and $X_yNi_xFe^{III}(CN)_6$, spectra of high quality at the *K*-edge of Fe can be obtained using fluorescence detection.

The EXAFS spectra have been fitted with the model of Ref. [37] and using the significant Multiple Scattering path specified in Section 2. Fig. 4 displays the comparison of the experimental and theoretical EXAFS signals (upper panel) and of the relative Fourier Transform (FT; bottom panel) of the two investigated compounds. From the same figure it is apparent that the theoretical signal matches well the experimental one, indicating the reliability of the chosen structural model and the accuracy of the data analysis conducted in both fitting procedures.

Fig. 5 displays the details of the EXAFS analysis in term of two and three body contribution to the total theoretical signals. It is apparent that the two-body $\gamma^{(2)}$ Fe–C and the three-body $\eta_1^{(3)}$ Fe–C–N, are very important in the determining the total theoretical one in the whole range of analysed frequency. It is worth noting that the large amplitude of the three-body signal has been already observed in hexacyanoferrate materials and it is due to the focusing effect [37]. The residual appears to be very low and accounts for a high-frequency contribution not included in the calculation (see below). This contribution should arise from the four-body signal Fe–C–N–Ni [37], since the nickel hexacyanoferrate is structurally characterized by a framework of atomic linear chain –Fe–C–N–Ni–. Moreover, the experimental FT curves displayed in Fig. 4 actually show, in both Ni/Al–$Fe^{III}(CN)_6$ and

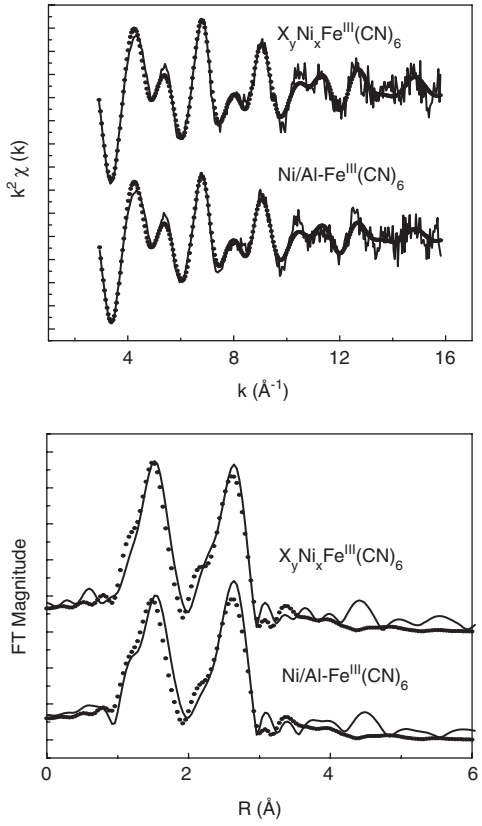

Fig. 4. EXAFS analysis at the Fe *K*-edge (7112 eV) of Ni/Al–$Fe^{III}(CN)_6$ and $X_yNi_xFe^{III}(CN)_6$ compounds. The upper panel displays the comparison of the total theoretical signal (solid line) with the experimental one (dot line) of the EXAFS spectra, performed over the range $k = 2.9$–15.9 Å^{-1}. The lower panel shows the comparison of the total theoretical signal (solid line) with the experimental one (dot line) of the corresponding Fourier Transforms (FT).

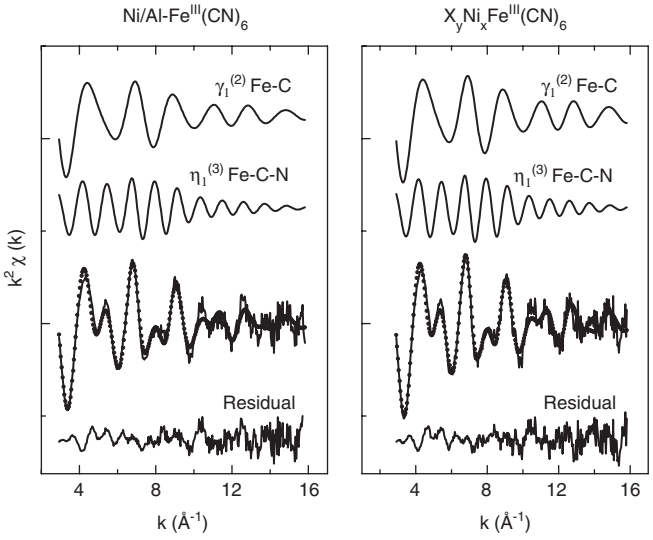

Fig. 5. Details of the EXAFS analysis at the Fe *K*-edge (7112 eV) of Ni/Al–$Fe^{III}(CN)_6$ and $X_yNi_xFe^{III}(CN)_6$ compounds. The figure shows the individual EXAFS contributions, in terms of two- and three-body signals. In the middle, the comparison of the total theoretical signal (solid line) with the experimental (dot line) is illustrated. The residual is shown at the bottom.

$X_yNi_xFe^{III}(CN)_6$ spectra, a contribution at about 4.5 Å, which corresponds to a high-frequency signal in the EXAFS spectrum. The attempt of including this four-body contribution in the data analysis did not improve significantly the fitting.

Table 1 summarize the obtained structural parameters of the Ni/Al–$Fe^{III}(CN)_6$ and [$X_yNi_xFe^{III}(CN)_6$] as obtained by the EXAFS best fits. The fit outcome indicates that the first shell Fe–C in the intercalated Htlc is slightly shorter (0.05 Å) than the values observed for the crystalline forms or the solutions of hexacyanoferrates [47], but in agreement with cobalt hexacyanoferrates intercalated in silica matrix [48]. The C≡N bond distance is seen to be in line with the value normally quoted for this class of compounds. The fitting procedure has also permitted to check the possible structural modification upon the exchange process (comparison of the Ni/Al–$Fe^{III}(CN)_6$ with $X_yNi_xFe^{III}(CN)_6$). As seen from Table 1, the relevant structural parameters of the two samples are found to be almost the same, apart of a slight decrease of the EXAFS bond variance of Fe–C, indicating the preservation of the overall structure.

This issue is also confirmed comparing the XANES spectra taken at the Fe *K*-edge of Ni/Al–$Fe^{III}(CN)_6$ and $X_yNi_xFe^{III}(CN)_6$ compounds, shown in Fig. 6. As seen, the two curves are very similar with differences visible in the pre-edge region (P_1) as well as in the main peak region (P_2) directly associated to transitions to empty bound states [49] that deals with the local coordination geometry of the photo-absorber, and on the intensity of the first EXAFS oscillation, at about 7140 eV, that reflects the low EXAFS bond variance of the first coordination shell Fe–C, already observed by the EXAFS analysis.

Table 1
Selected structural parameters from EXAFS fitting results[a] of Ni/Al–$Fe^{III}(CN)_6$ and $X_yNi_xFe^{III}(CN)_6$

	Ni/Al–$Fe^{III}(CN)_6$	$X_yNi_xFe^{III}(CN)_6$
Fe–C bond distance/Å	1.89	1.89
σ^2 Fe–C/Å^2	0.003	0.002
C≡N bond distance/Å	1.18	1.18
σ^2 C≡N/Å^2	0.011	0.010

[a]The error associated with each bond length is 0.01 Å.

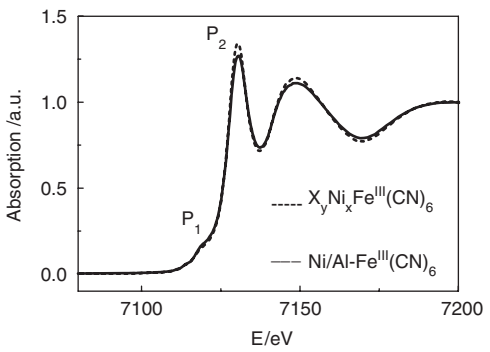

Fig. 6. Comparison of XANES spectra of Ni/Al–$Fe^{III}(CN)_6$ and $X_yNi_xFe^{III}(CN)_6$ taken at the Fe *K*-edge (7112 eV). Spectra were taken using fluorescence detection.

3.1.4. Electrochemical measurements

The work by Zamponi et al. [50] has clearly demonstrated that the electrochemical properties of NiHCF are strongly dependent on the method of preparation, exposure and concentration of the electrolyte cation K^+. The multipeak voltammetry of K^+ intercalation/deintercalation has been tied to NiHCF stoichiometry.

Specifically, the lower voltage CV peaks occurred in films that were lower in potassium, while higher voltage CV peaks occurred in film that were richer in potassium. For the two predominant forms of electrodeposited NiHCF films the following approximate formulas can be assigned: $XNi_{1.5}[Fe^{II}(CN)_6]$ and $X_2Ni[Fe^{II}(CN)_6]$ (where X^+ is Li^+, Na^+ or K^+). Assuming charge propagation is provided through the flux of cations, the system's redox reactions can be written as

$$Ni_{1.5}[Fe^{III}(CN)_6] + e^- + X^+ \rightleftarrows XNi_{1.5}[Fe^{II}(CN)_6] \quad (1)$$

$$XNi[Fe^{III}(CN)_6] + e^- + X^+ \rightleftarrows X_2Ni[Fe^{II}(CN)_6] \quad (2)$$

The actual stoichiometries of NiHCF are dependent on the nature of alkali metal cation, and they are likely to be differently composed of "insoluble" (K^+-free), "soluble" (K^+-rich) or defective structural analogues of nickel-substituted Prussian Blue [51].

The structural analogue of soluble Prussian Blue has an ideal Ni:Fe stoichiometry of unity; higher Ni:Fe ratios arise from $Fe(CN)_6^{4-}$ lattice vacancies, extra Ni^{2+} occupying interstitial alkali cation sites. Therefore, the higher voltage peak arises from the nearly perfect 1:1 stoichiometry, whereas the lower voltage CV peak from the non-stoichiometric structure.

Fig. 7 shows the cyclic voltammetry of the compound $X_yNi_xFe^{III}(CN)_6$ in a 0.1 M tetraethylammonium perchlorate (TEAP) solution in order to obtain informations on the dynamics of ions insertion/release.

Although the supporting electrolyte does not contain potassium ions, the system is characterized by the couples of anodic and cathodic peaks typical of mixed hexacyanoferrates, obtained during the electrodeposition of a NiHCF film from a solution containing K^+ salts,

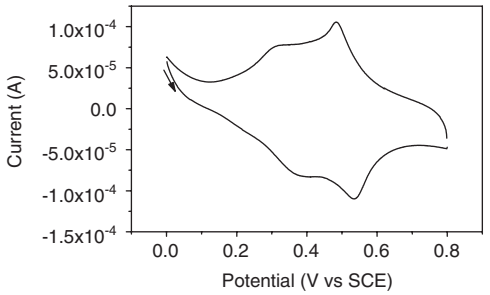

Fig. 7. Cyclic voltammetry recorded in 0.1 M TEAP solution for the solid $X_yNi_xFe^{III}(CN)_6$. Scan rate: 0.01 V s^{-1}.

as stated above [50]. As already observed [33] a possible explanation of these experimental findings is the occurrence of the intercalation of the ion-pair potassium—hexacyanoferrate inside the parent Htlc. The contact with the Ni^{2+} solution promotes the formation of a NiHCF where the interstitial holes are occupied by K^+, due to the strong affinity of potassium ions for metal hexacyanoferrates [27].

As to the K^+ absence/presence issue, the CV test appears to be definitive while Raman and FT-IR analysis had failed in confirming this evidence.

The elemental analysis performed on $X_yNi_xFe^{III}(CN)_6$ made this hypothesis more conclusive, as revealed by the presence of potassium. On the basis of the data obtained, the following approximate stoichiometric formula $K_{0.8}Ni_{1.1}Fe^{III}(CN)_6$ was proposed. The ratio Ni:Fe close to 1 is indicative of a K^+-rich structure.

3.2. Evidence of K^+-free nickel hexacyanoferrate

As stated before, FT-IR and Raman spectroscopy suggested the occurrence of the compounds $KNiFe^{III}(CN)_6$ or $HNiFe^{III}(CN)_6$ in the intercalated Htlc, although their presence was not confirmed by XRD, probably because the crystalline domains were too small to be observed. In order to check for the pure mixed hexacyanoferrate, a sample of intercalated Htlc (60 mg) was solubilized with 1 M HCl (70 mL). The acid treatment left a solid residue, which was separated by centrifugation, washed with doubly distilled water and dried under vacuum in an oven (50 °C). The obtained material (8.3 mg) was characterized by means of XRD, cyclic voltammetry and ICP-OES.

The XRD spectrum (Fig. 8) displays a broad pattern with only a single maximum, due to the diffraction by the basal plane (200), which can be ascribed to the compounds $KNiFe^{III}(CN)_6$ or $Ni_3[Fe(CN)_6]_2 \cdot 10H_2O$. Due to the large structural disorder, the other reflections were not observed.

The electrochemical measurements were performed in 0.5 M KNO_3 solution, directly on the powder mechanically attached to a gold disk [50] and the corresponding curves are displayed in Fig. 9. The first cycle (Fig. 9A) was

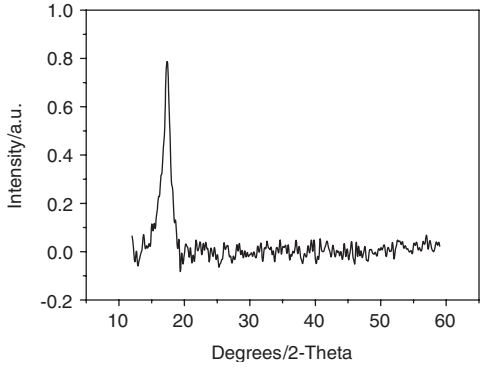

Fig. 8. XRD pattern of the product obtained after HCl treatment.

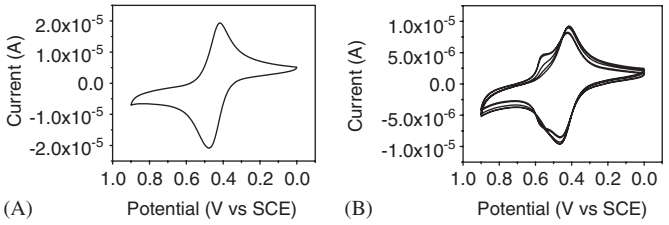

Fig. 9. Cyclic voltammetry (9A: first cycle; 9B: after 20 cycles) recorded in 0.5 M KNO_3 solution for the solid obtained by dissolving the intercalated Htlc Ni/Al–$Fe^{III}(CN)_6$ in 1 M HCl. Scan rate: 0.05 V s^{-1}.

dominated by a typical reversible couple of peaks. When performing further cycles in potassium salt electrolyte, the system started to show an additional peak at higher potentials (Fig. 9B). These findings could be explained as follows. Nickel-rich NiHCF compounds, characterized by relatively high ratios of Ni to Fe and by very small amounts of interstitial K^+, display only a single set of peaks at relatively negative potentials [50]. On the contrary, the exposure of such a structure to K^+ salt electrolytes results in the uptake of potassium ions producing the so-called K^+-rich NiHCF, with the subsequent appearance of the higher voltage peak system in CV.

ICP-OES analysis of the solid obtained after HCl treatment, performed after its solubilization in 1 M LiOH confirms the absence of potassium. Hence, we refer to such a material as K^+-free nickel hexacyanoferrate. The molar ratio of Ni:Fe resulted 1.7 ± 0.3, in agreement with a pure nickel hexacyanoferrate, leading to the formula $Ni_{1.5}Fe^{III}(CN)_6$. Therefore, the intercalation of $Fe(CN)_6^{3-}$ inside a synthetic Htlc, containing Ni as bivalent metal, and its dissolution in HCl revealed a good strategy to obtain the K^+-free nickel hexacyanoferrate, with a yield of about 14%.

4. Conclusions

Experimental results confirmed the synthesis of a nickel hexacyanoferrate as demonstrated with the combined use of XRD, FT-IR, Raman and XAS spectroscopy. In addition, electrochemical analysis and ICP-OES provided the evidence for the absence of potassium, i.e., the formation of K^+-free nickel hexacyanoferrate. The synthesis proposed in this work uses a Ni/Al hydrotalcite as host material for the intercalation of hexacyanoferrate(III). To obtain the K^+-free nickel hexacyanoferrate, the Htlc host was further dissolved in acid solution. Due to the different solubility of Htlc and NiHCF compounds in acid solutions it was possible to obtain K^+-free nickel hexacyanoferrate with a yield of 14%. Though not further improved, the approach here described appears well-suitable for scaling up to larger amounts of material, since a better yield in the synthesis of the host material Ni/Al–$Fe^{III}(CN)_6$ is an affordable target for achieving this goal.

Acknowledgments

Measurements at Daresbury Laboratory were supported by the European Community–Research Infrastructure Action under the FP6 "Structuring the European Research Area" Programme (through the Integrated Infrastructure Initiative "Integrating Activity on Synchrotron and Free Electron Laser Science").

References

[1] R.L. Frost, A.W. Musumeci, J. Bouzaid, M.O. Adebajo, W.N. Martens, J.T. Kloprogge, J. Solid State Chem. 178 (2005) 1940.
[2] J.W. Boclair, P.S. Braterman, B.D. Brister, Z. Wang, F. Yarberry, J. Solid State Chem. 161 (2001) 249.
[3] A. Dostal, M. Hermes, F. Scholz, J. Electroanal. Chem. 415 (1996) 133 (and references therein).
[4] M.K. Carpenter, R.S. Conell, J. Electrochem. Soc. 137 (1990) 2464.
[5] E.A.R. Duek, M.A. De Paoli, M. Mastragostino, Adv. Mater. 4 (1992) 287.
[6] P.M.S. Monk, R.J. Mortimer, D.R. Rosseinsky, Electrochromism, Fundamentals and Applications, VCH, Weinheim, 1995 (Chapter 6).
[7] P.J. Kulesza, M.A. Malik, M. Berrettoni, M. Giorgetti, S. Zamponi, R. Schmidt, R. Marassi, J. Phys. Chem. B 102 (1989) 1870.
[8] S.S. Narayanan, F. Scholz, Electroanalysis 11 (1999) 465.
[9] A.A. Karyakin, E.E. Karyakina, Electrochem. Commun. 1 (1999) 78.
[10] D.M. Zhou, H.X. Ju, H.Y. Chen, J. Electroanal. Chem. 408 (1998) 219.
[11] V.D. Neff, J. Electrochem. Soc. 132 (1985) 1382.
[12] M. Kaneko, T. Okada, J. Electroanal. Chem. 255 (1988) 45.
[13] M. Jayalakshmi, F. Scholz, J. Power Sources 87 (2000) 212.
[14] P.J. Kulesza, J. Electroanal. Chem. 289 (1990) 103.
[15] M. Pyrasch, A. Toutianoush, W.Q. Jin, J. Schnepf, B. Tieke, Chem. Mater. 15 (2003) 245.
[16] O. Sato, T. Iyoda, A. Fujishima, K. Hashimoto, Science 272 (1996) 704.
[17] O. Sato, Y. Einaga, T. Iyoda, A. Fujishima, K. Hashimoto, J. Phys. Chem. B 101 (1997) 3903.
[18] A. Bleuzen, C. Lomenech, V. Escax, F. Villain, F. Varret, C. Cartier dit Moulin, M. Verdaguer, J. Am. Chem. Soc. 122 (2000) 6648.
[19] C. Mingotaud, C. Lafuente, J. Amiell, P. Delhaes, Langmuir 15 (1999) 289.
[20] C.A. Lundgren, R.W. Murray, Inorg. Chem. 27 (1988) 933.
[21] N. Toshima, K. Liu, M. Kaneko, Chem. Lett. (1990) 485.
[22] S.D. Rassat, J.H. Sukamoto, R.J. Orth, M.A. Lilga, R.T. Hallen, Sep. Purif. Technol. 15 (1999) 207.
[23] Z. Deng, W.H. Smyrl, J. Electrochem. Soc. 138 (1991) 1911.
[24] R.J. Mortimer, P.J.S. Barbeira, A.F.B. Sene, N.R. Stradiotto, Talanta 49 (1999) 271.
[25] R. Koncki, Crit. Rev. Anal. Chem. 32 (2002) 79.
[26] A.A. Karyakin, Electroanalysis 13 (2001) 813.
[27] M. Giorgetti, E. Scavetta, M. Berrettoni, D. Tonelli, Analyst 126 (2001) 2168.
[28] F. Scholz, A. Dostal, Angew. Chem. Int. Ed. Engl. 34 (1995) 2685.
[29] J. Joseph, H. Gomathi, G. Prabhakara Rao, Electrochim. Acta 36 (1991) 1537.
[30] N.R. de Tacconi, K. Rajeshwar, R.O. Lezna, Chem. Mater. 15 (2003) 3046.
[31] J. Bacskai, K. Martinusz, E. Czirok, G. Inzelt, P.J. Kulesza, M.A. Malik, J. Electroanal. Chem. 385 (1995) 241.
[32] W.A. Steen, D.T. Schwartz, Chem. Mater. 15 (2003) 2449.
[33] I. Carpani, M. Berrettoni, B. Ballarin, M. Giorgetti, E. Scavetta, D. Tonelli, Solid State Ion. 168 (2004) 167.
[34] S. Miyata, Clays Clay Min 31 (1983) 305.
[35] A. Filipponi, A. Di Cicco, C.R. Natoli, Phys. Rev. B 52 (1995) 15122.
[36] A. Filipponi, A. Di Cicco, Phys. Rev. B 52 (1995) 15135.
[37] M. Giorgetti, M. Berrettoni, A. Filipponi, P.J. Kulesza, R. Marassi, Chem. Phys. Lett. 275 (1997) 108.
[38] L. Hedin, B.I. Lundvquist, J. Phys. C 4 (1971) 2064.
[39] M. Krause, J.H. Oliver, J. Phys. Chem. Ref. Data 8 (1979) 329.
[40] M.J. Holgado, V. Rives, M.S. Sanromán, P. Malet, Solid State Ion. 92 (1996) 273.
[41] K.M. Jeerage, W.A. Steen, D.T. Schwartz, Chem. Mater. 14 (2002) 530.
[42] I. Carpani, M. Berrettoni, M. Giorgetti, D. Tonelli, J. Phys. Chem. B 110 (2006) 7265.
[43] A. Filipponi, J. Phys.: Condens. Matter 13 (2001) R23.
[44] E. Frabetti, G.A. Deluga, W.H. Smyrl, M. Giorgetti, M. Berrettoni, J. Phys. Chem. B 108 (2004) 3765.
[45] M. Giorgetti, S. Passerini, W.H. Smyrl, M. Berrettoni, Chem. Mater. 11 (1999) 2257.
[46] M. Giorgetti, S. Mukerjee, S. Passerini, J. McBreen, W.H. Smyrl, J. Electrochem. Soc. 148 (2001) A768.
[47] K. Hayakawa, K. Hatada, P. D'Angelo, S. Della Longa, C.R. Natoli, M. Benfatto, J. Am. Chem. Soc. 126 (2004) 15618.
[48] M. Giorgetti, M. Berrettoni, S. Zamponi, P.J. Kulesza, J.A. Cox, Electrochim. Acta 51 (2005) 511.
[49] P. Cecchi, M. Berrettoni, M. Giorgetti, G. Gioia Lobbia, S. Calogero, L. Stievano, Inorg. Chim. Acta 318 (2001) 67.
[50] S. Zamponi, M. Berrettoni, P.J. Kulesza, K. Miecznikowski, M.A. Malik, O. Makowski, R. Marassi, Electrochim. Acta 48 (2003) 4261.
[51] Q. Yu, W.A. Steen, K.M. Jeerage, S. Jiang, D.T. Schwartz, J. Electrochem. Soc. 149 (2002) E195.